IJESRT

INTERNATIONAL JOURNAL OF ENGINEERING SCIENCES & RESEARCH TECHNOLOGY

A NUMERICAL INVESTIGATION OF TURBULENT NATURAL CONVECTION IN A 3-D ENCLOSURE USING *K-ω* SST MODEL AND SIMPLEC METHOD

Kimunguyi Kiliswa Josephs*[1], Grace Wambui Gachigua[2] & Francis Kimani Gatheri[3]
*[1]P.O. Box 444 – 00206, Kiserian, Kenya
[2&3]School of Mathematics and Actuarial Science, Technical University of Kenya

ABSTRACT

The objective of this study is to conduct a numerical investigation of turbulent natural convection in a 3-D cavity using the k-ω SST model and the SIMPLEC method. The statistical-averaging process of the mass, momentum and energy governing equations introduces unknown turbulent correlations into the mean flow equations which represent the turbulent transport of momentum, heat and mass, namely Reynolds stress $(\overline{u_i u_j})$ and heat flux $(\overline{u_i \theta})$, which are modelled using k-ω SST model. The Reynolds-Averaged Navier-stokes (RANS), energy and k-ω SST turbulent equations are first non-dimensionalized and the resulting equations are discretized using Finite Volume Method and solved using SIMPLEC. From the results,both the experimental data and simulation using SIMPLEC return a non-dimensional temperature of 0.5 at the core of the cavity and almost zero towards the cold and the natural turbulence flow is responsible for temperature distribution.

KEYWORDS: Turbulence, natural Convention, k-ω SST, SIMPLEC Method.

I.   INTRODUCTION

In fluid dynamics, turbulence is a flow regime characterized by chaotic and stochastic changes. This includes low momentum diffusion, high momentum convection and rapid variation of pressure and velocity in space and time. Turbulent flows exist everywhere in nature from the jet stream to the oceanic currents. Turbulent flows are highly irregular and random which makes a deterministic (predictable) approach to turbulence problems impossible.

II.   MATHEMATICAL FORMULATION

In this thesis, a numerical investigation of turbulent natural convection within a 3-D is conducted. The geometry is illustrated in figure 3.1. It consists of a hot surface, located on the left side of the rectangular cavity wall, and a cold surface on the right side. The enclosure is heated on the hot wall (Red color) and cooled on the cold wall (blue color).The measurement of Ampofo and Karyiannis (2003) were used. The walls measures 0.75m by 0.75m wide by 1.5m. The hot and cold walls of the cavity were isothermal at 323 ± 0.15K and 283 ± 0.15K respectively, giving a Reyleigh number of 1.58×10^9. Each of the remaining walls are adiabatic. All boundaries of the enclosure are stationary, non-slip, rigid and impermeable.

Initially, the fluid is motionless the temperature of which is equal to the average temperature of the vertical walls. Let the temperature of the heater be T_h and that of the window be T_w. The temperature of the heater and that of the window are varied such that $T_h > T_w$. This implies that the density gradient of the internal fluid is normal to the gravity and the buoyancy–driven natural convection starts immediately the heat is applied. Due to the buoyancy, a fluid motion is induced in the enclosure depending on the enclosure geometry (i.e. aspect ratio A=H/L), the working fluid (air) and temperature difference ΔT.

The fluid to be used is air. Therefore fluid flow will depend only on the temperature difference given as $\Delta T = T_h - T_w$. Aspect ratio A=H/L=0.5, Where H is the height and L is the Length of the enclosure. The characteristic length is taken to be the size of the enclosure in the $x-$ direction. Furthermore, the Boussinesq Approximation (1903) is assumed and is presented below.

In this research, we will zero in on the standard $\kappa - \omega\ SST$ turbulence models as documented by Awuor (2012) and study the variables as used by Ampofo and Karyiannis (2003).
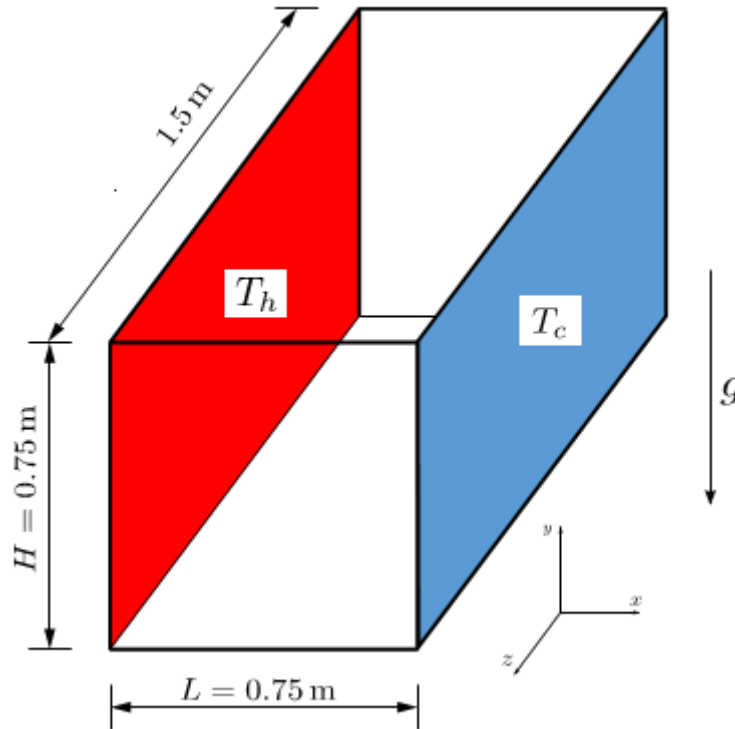

Fig. 2.1   Geometry of the 3-D numerical model

III.   GOVERNING EQUATIONS

The equations governing the flow of incompressible Newtonian fluid are derived from equations, which enforce the conservation of mass, the conservation of momentum, and conservation of energy. The equation of continuity, the momentum equation and the energy equation are given as equations (3.1), (3.2) and (3.3) below respectively:

$$\frac{\partial \rho}{\partial t} + \frac{\partial}{\partial x_j}(\rho u_j) = 0 \tag{3.1}$$

$$\frac{\partial}{\partial t}\rho u_j + \frac{\partial}{\partial x_j}\rho u_i u_j = -\frac{\partial P}{\partial x_i} + \rho g_i + \frac{\partial}{\partial x_j}\left[\mu\left(\frac{\partial u_i}{\partial x_j} + \frac{\partial u_j}{\partial x_i}\right) + \mu_s \delta_{ij}\frac{\partial u_k}{\partial x_k}\right] \tag{3.2}$$

Where μ and μ_s are the first and second coefficient of viscosity.

$$\frac{\partial}{\partial t}(C_P \rho T) + \frac{\partial}{\partial x_j}(C_P \rho u_j T) = \frac{\partial}{\partial x_j}\left(\lambda\frac{\partial T}{\partial x_j}\right) + \beta T\left(\frac{\partial p}{\partial t} + \frac{\partial u_j p}{\partial x_j}\right) + \Phi \tag{3.3}$$

IV.   TURBULENCE MODELING

Reynolds Decomposition
The concept entails decomposing the instantaneous fluid flow quantities (variables) in the Navier-Stokes equations into mean (time-averaged) value and fluctuating value.

Instantaneous Equations of Motion
A turbulent flow instantaneously satisfies the Navier-Stokes equations and the equations of motion for the instantaneous variables are;

$$\frac{\partial \tilde{\rho}}{\partial t} + \frac{\partial}{\partial x_i}(\tilde{\rho}\tilde{u}_j) = 0 \qquad (4.1)$$

$$\frac{\partial}{\partial t}\tilde{\rho}\tilde{u}_j + \frac{\partial}{\partial x_j}\tilde{\rho}\tilde{u}_i\tilde{u}_j = -\frac{\partial \tilde{P}}{\partial x_i} + \tilde{\rho}g_i + \frac{\partial}{\partial x_j}\left[\mu\left(\frac{\partial \tilde{u}_i}{\partial x_j} + \frac{\partial \tilde{u}_j}{\partial x_i}\right) + \mu_s\delta_{ij}\rho\frac{\partial \tilde{u}_k}{\partial x_k}\right] \qquad (4.2)$$

$$\frac{\partial}{\partial t}\left(\tilde{C}_P\tilde{\rho}\tilde{T}\right) + \frac{\partial}{\partial x_j}\left(\tilde{C}_P\tilde{\rho}\tilde{U}_j\tilde{T}\right) = \frac{\partial}{\partial x_j}\left(\lambda\frac{\partial \tilde{T}}{\partial x_j}\right) + \beta T\left(\frac{\partial \tilde{p}}{\partial t} + \frac{\partial \tilde{u}_j\tilde{p}}{\partial x_j}\right) + \Phi \qquad (4.3)$$

The equations satisfied by the mean flow are obtained by substituting the Reynolds decomposition into the instantaneous Navier-Stokes equations and taking the average of the equations

Averaged Equations of Motion
   a)   Continuity equation for Turbulent flow
Decomposing the instantaneous differential form of the continuity equation (4.2) into its mean and turbulent part, taking the time average and simplifying yields;

$$\frac{\partial \bar{\rho}}{\partial t} + \frac{\partial}{\partial x_j}\left(\bar{\rho}\bar{u}_j + \overline{\rho'u_j'}\right) = 0 \qquad (4.4)$$

   b)   Momentum Equation for Turbulent Flow
Decomposing the instantaneous dependent variables of the momentum equation, taking the average, expanding and then simplifying this equation yields:-

$$\overline{\frac{\partial}{\partial x_j}\left[\mu\left(\frac{\partial(\bar{u}_i + u_i')}{\partial x_j} + \frac{(\bar{u}_j + u_j')}{\partial x_i}\right) + \mu_s\delta_{ij}\rho\frac{\partial(\bar{u}_k + u_k')}{\partial x_k}\right]} = \frac{\partial}{\partial x_j}\left[\mu\left(\frac{\partial\bar{u}_i}{\partial x_j} + \frac{\partial\bar{u}_j}{\partial x_i}\right) + \mu_s\delta_{ij}\frac{\partial\bar{u}_k}{\partial x_k}\right] \qquad (4.5)$$

The correlation $\overline{u_iu_j}$ in equation (4.5) is generally nonzero.
   (a)   Mean Heat Equation
Decomposing the instantaneous temperature variable in the heat equation into the mean part and the deviation from the mean, and simplifying this equation yields;

$$\frac{\partial}{\partial t}\left(C_P\bar{\rho}\bar{T} + C_P\overline{\rho'T'}\right) + \frac{\partial}{\partial x_j}\left(C_P\overline{\rho u_j}\bar{T}\right)$$
$$= \frac{\partial\bar{p}}{\partial t} + \frac{\partial\bar{p}}{\partial x_j} + \overline{u_i'\frac{\partial p'}{\partial x_j}} + \frac{\partial}{\partial x_j}\left(\lambda\frac{\partial\bar{T}}{\partial x_j} - C_P\bar{\rho}\overline{u_i'T'} - C_P\overline{\rho'u_iT'}\right) + \bar{\Phi} \qquad (4.6)$$

Where;

$$\bar{\Phi} = \overline{\tau_{ij}}\frac{\partial\bar{u}_i}{\partial x_j} + \overline{\tau'_{ij}\frac{\partial u_i'}{\partial x_j}} \qquad (4.7)$$

V.   NON-DIMENSIONALISATION

This implies the partial or full removal of units from an equation involving physical quantities by a suitable substitution of variables. This technique can simplify and parametize problems where measured units are involved. The reesulting equations in general form become;

$$\frac{\partial\rho}{\partial t} + \frac{\partial}{\partial x_j}\left(\rho U_i + \overline{\rho u_j}\right) \qquad (5.1)$$

$$\frac{\partial}{\partial t}\left(\rho U_i + \overline{\rho u_i}\right) + \frac{\partial}{\partial x_j}\left(\rho U_iU_j + U_i\overline{\rho u_j}\right) = -N_1\frac{\partial P}{\partial x_i} + N_2 pg_i + \frac{\partial}{\partial x_j}\left(N_3\tau_{ij} - U_i\overline{\rho u_i} - \rho\overline{u_iu_j} - \overline{\rho u_iu_j}\right)$$
$$= 0 \qquad (5.2)$$

$$\frac{\partial}{\partial t}(c_P\rho\Theta + c_P\overline{\rho\Theta}) + \frac{\partial}{\partial x_j}\left(c_P\overline{\rho U_j\Theta}\right)$$

$$= L_1\left[\frac{\partial p}{\partial t} + U_j\frac{\partial p}{\partial x_j} + \overline{u_j\frac{\partial p}{\partial x_j}}\right] + \frac{\partial}{\partial x_j}\left(L_2\lambda\frac{\partial\Theta}{\partial x_j} - c_P\overline{\rho\Theta} + c_P\rho\Theta\right)$$

$$+ L_3\emptyset \tag{5.3}$$

$$\frac{\partial}{\partial t}\rho k + \frac{\partial}{\partial x_j}(\rho U_i k) = A_1\overline{u_j\frac{\partial\mu}{\partial x_j}}\left(\frac{\partial u_i}{\partial x_j} + \frac{\partial u_j}{\partial x_i}\right) - \frac{1}{2}\frac{\partial}{\partial x_j}\overline{\rho u_i u_j}\frac{\partial U_i}{\partial U_j} + B_2\overline{\rho u_i}g_i - B_3\overline{u_j\frac{\partial p}{\partial x_i}} \tag{5.4}$$

$$\frac{\partial}{\partial t}\rho\omega + \frac{\partial}{\partial x_j}(\rho U_j\omega)$$

$$= -\frac{\partial}{\partial x_k}\left(\overline{B_1\mu u_k\frac{\partial u_i}{\partial x_j}\frac{\partial u_i}{\partial x_j}} + 2B_2\nu\frac{\partial u_k}{\partial x_i}\frac{\partial u_\rho}{\partial x_i} - B_1\mu\frac{\partial\omega}{\partial x_k}\right)$$

$$- 2B_1\mu\frac{\partial U_i}{\partial x_j}\left(\frac{\partial u_i}{\partial x_j}\frac{\partial u_k}{\partial x_j} + \frac{\partial u_j}{\partial x_j}\frac{\partial u_j}{\partial x_k}\right) - 2B_1\mu\frac{\partial^2 U_i}{\partial x_j\partial x_k}\overline{\mu_k\frac{\partial u_i}{\partial x_j}} \tag{5.5}$$

VI.   METHOD OF SOLUTION

The SIMPLEC Solution Algorithm
The SIMPLEC Algorithm follows the same steps as SIMPLE algorithm, with the difference that the momentum equations are manipulated so that the SIMPLEC velocity correction equations omit terms that are less significant than those omitted in SIMPLE.
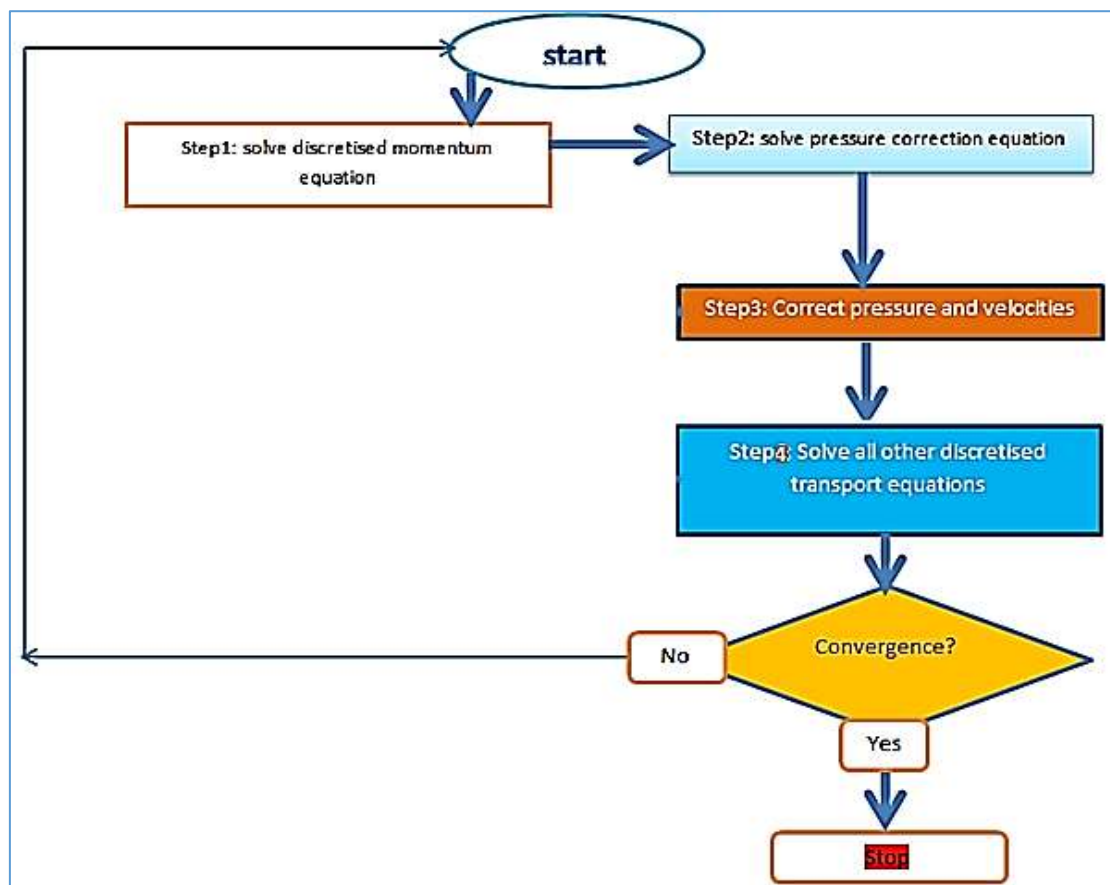
SIMPLEC Flow Chart

Fig 6.1 SIMPLEC Algorithm flow chart

VII. RESULTS AND DISCUSSION

The results presented here were obtained by solving equations (5.1), (5.2), (5.3), (5.4) and (5.5) by SIMPLEC algorithm after discretization as shown in flow chart (6.1) and together with the boundary conditions gave the following numerical solutions. The numerical results we have found were validated against the experimental data provided by Ampofo and Karayiannis (2003). This benchmark is at a Rayleigh number of 1.58×10^9.
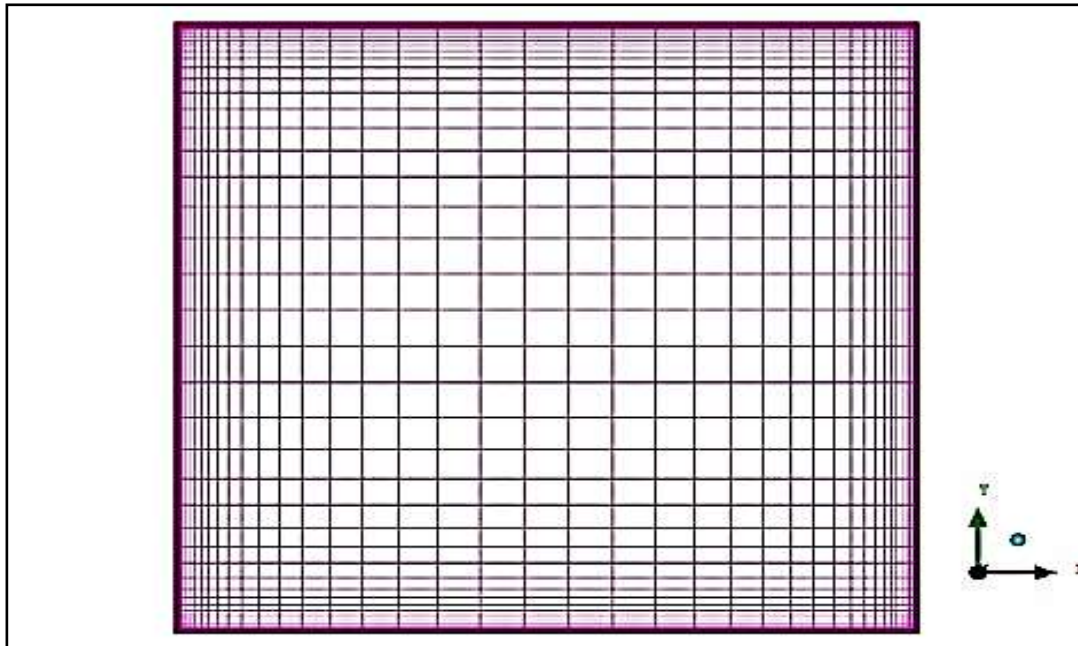
Grid and Grid Convergence

Fig 7.1 grid 80x80

The grid shown in figure 7.1 above is the standard grid used in these validations. The computational grids are staggered and clustered towards the walls.

Grids are staggered so that the scalar variables like pressure, temperature, density and turbulent quantities are stored in the cell centers of the control volume whereas vector variables like velocity and momentum are located in the cell faces. All variables are calculated right up to the walls without using any wall function since the $k - \omega \, SST$ model would use its blending function to switch the model to the $k - \omega$ model which is more accurate and more numerically stable in the near wall regions. On the wall surface, the boundary values for the velocity components and the turbulent kinetic energy are set to zero in conformity with no slip boundary condition.
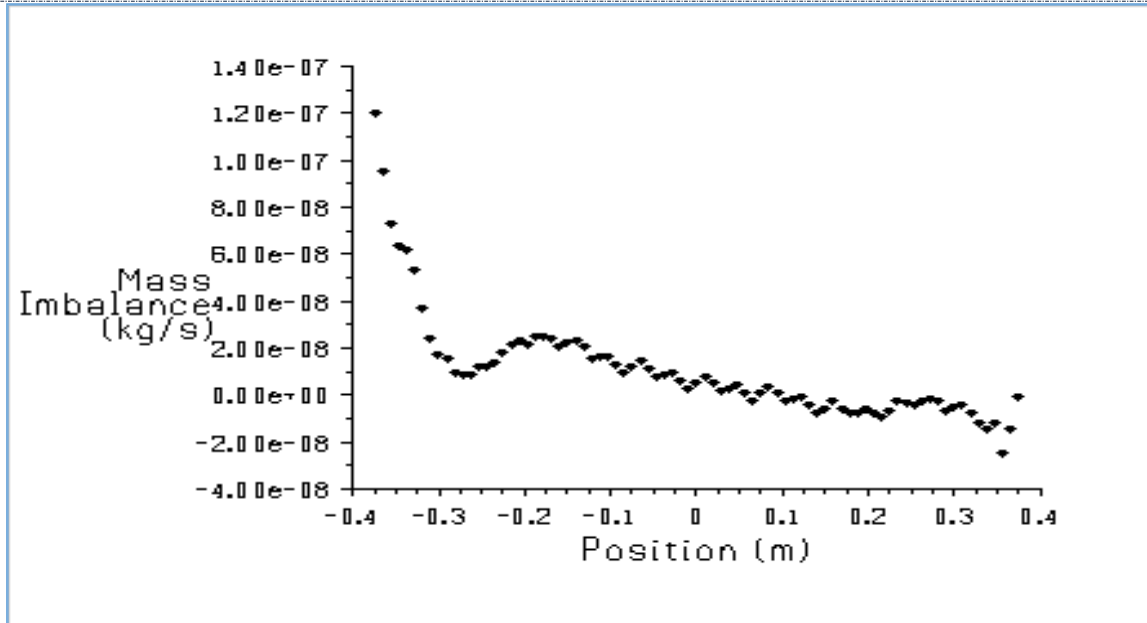
Fig 7.2   Mass imbalance profiles on an 80x80 grid

The dimensionless temperatures of the cold and hot walls are 0 and 1 respectively.

Firstly, we checked the solution for mesh convergence. This we did by carrying out a grid independence test. This was done by computing the numerical solution on successively finer grids. The difference in numerical solution between the coarse (80x80) and finer (160x160) grid, was to be taken as the accuracy measure of the coarse grid.

In this case, the 80x80 grid was refined by increasing the number of grid points to 160x160 for confirmation of grid independence. Figure 7.2 and Figure 7.3 show a comparison of the residual mass imbalance profiles for the flow generated on each of the grids. The numerical implication is that as the mesh spacing or control volume size approached zero, the discretized equation solution matches the exact solution.
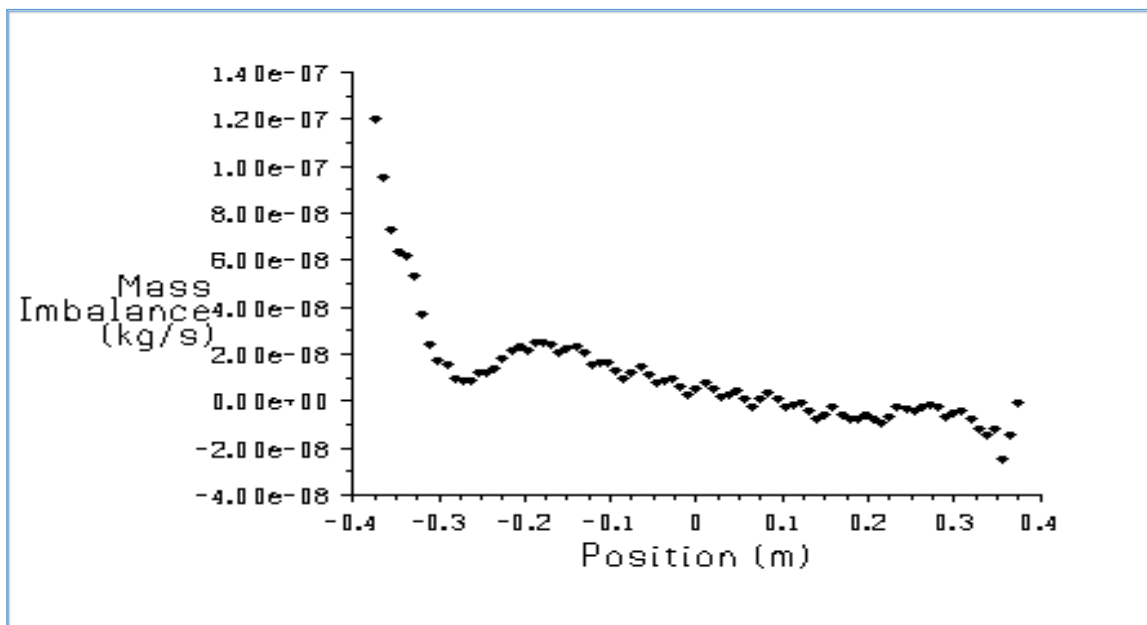

Fig 7.3 Mass imbalance grid on a 160x160 grid

Evidently, the results obtained on the 80x80 grid do not differ from those obtained on the 160x160 grid layout. Therefore, we can conclude the discretization error has diminished to zero and the grid independence has been reached.

Solution Convergence by SIMPLEC Method

Convergence was monitored with residuals, whereby a decrease in residuals by three orders of magnitude was to indicate at least qualitative convergence whereby case residual plots would show when the residual values have reached the specified tolerance.

A convergence of the root mean square residual of 1e-06 for energy and 1e-03 for turbulent kinetic energy, specific dissipation rate and $x-, y-$ and z – momentum equations, was sufficient for significant physical results, as shown in fig. 7.4. The residues had reduced to a sufficient degree.

The solution was to be deemed to have converged when the convergence criterion for each variable was reached. The default criterion was that each residual was to be reduced to a value of less than 10^{-3}, except the energy residual, for which the default criterion was 10^{-6}.
In this case too, under-relaxation was used to enable convergence except for density, energy and body forces. The values used ranged from 0.3 to 0.9.

For SIMPLEC, the residual convergence criterion for each variable was achieved and the residual imbalance became negligible after 350 iterations in a duration of 1hr, 15min.
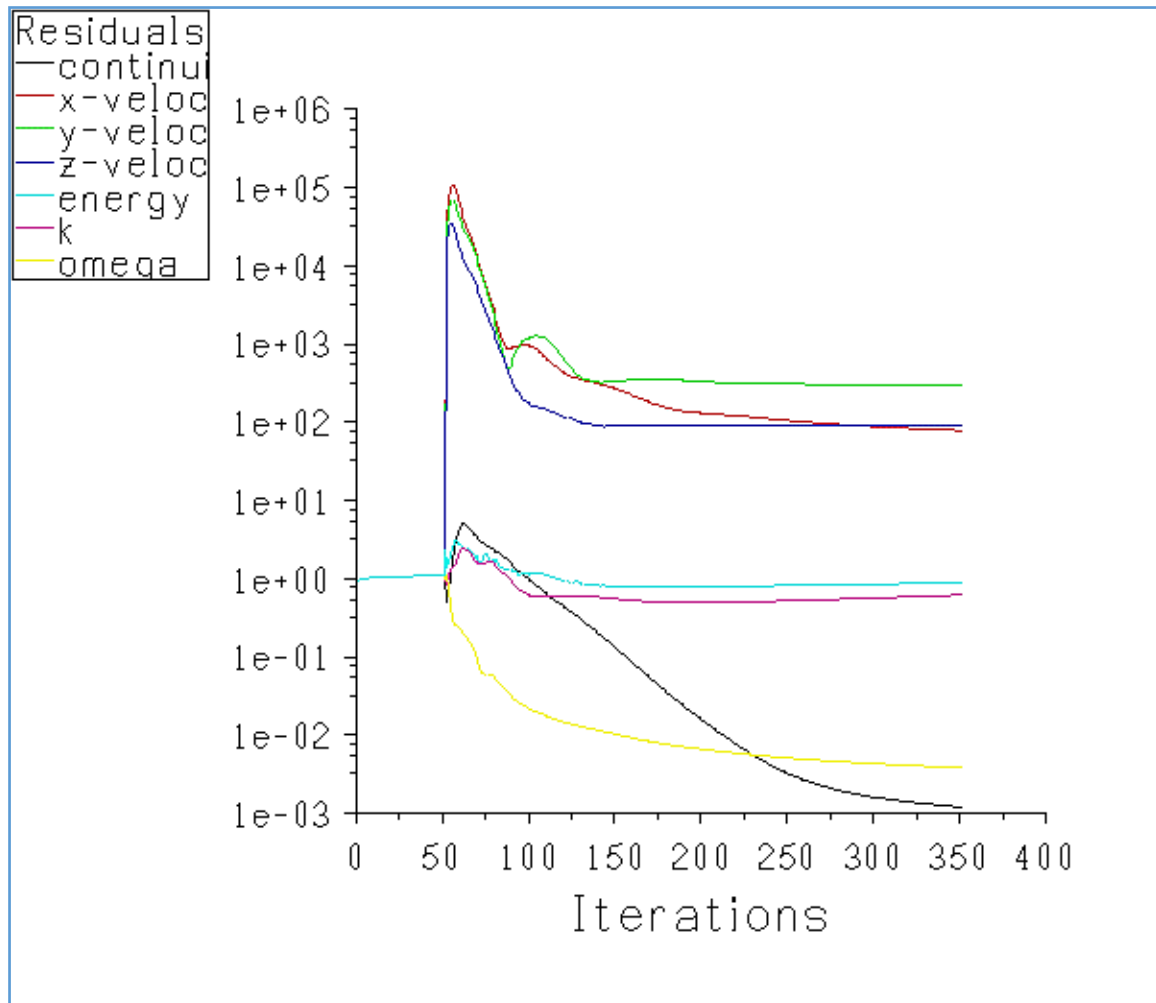

Fig 7.4 Scaled Residuals by SIMPLEC

Validation of Results

Verification and Validation to assess the accuracy and reliability of results in this numerical code was done against the experimental solutions obtained from Ampofo and Karayiannis (2003).
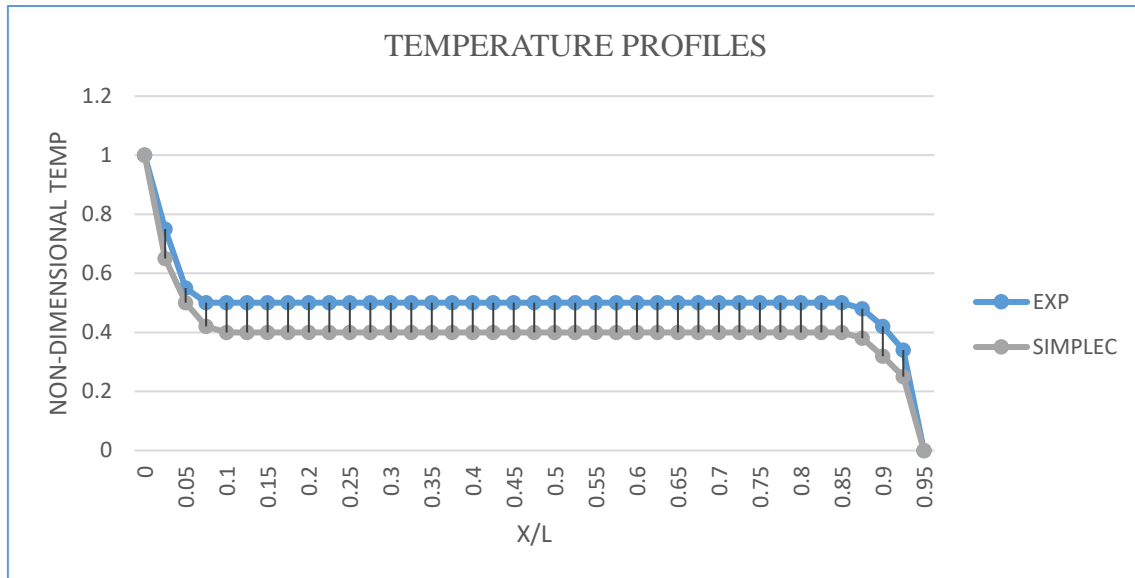
Temperature Profiles

Figure 7.5 Comparison of the Mean Temperature at y/H=0.5

From fig. 7.5, the mean temperature profiles show an almost uniform distribution in the enclosure core. This shows that in the enclosure core region, there is very little activity as the mean temperature is nearly uniform. The predicted temperatures by SIMPLEC show a minimum which is lower than the experimental values in the core of the cavity. This is due to a trace of the cold draft emanating from the opposite wall, which according to measurements, should have had time to totally mix while crossing over along the floor. Again this shows insufficient mixing with the laminar core. The SIMPLEC simulation yielded a temperature of 0.4 both at the center of the enclosure, and on the near wall profiles. In the enclosure core region, there is very little activity; the mean temperature is nearly uniform.

Turbulent Kinetic Energy profiles

These are a profile of the mean kinetic energy per unit mass, which are associated with root mean square fluctuating velocities in a turbulent flow. In this study, the turbulent kinetic energy is produced by shear, friction and buoyancy, transferred by turbulence energy cascade and dissipated by viscous forces (or molecular viscosity) at the Kolmogorov scales in the confluence. Fig. 7.6 displays the measured turbulent kinetic energy on the mid-width plane and the corresponding profiles obtained with SIMPLEC numerical simulations.
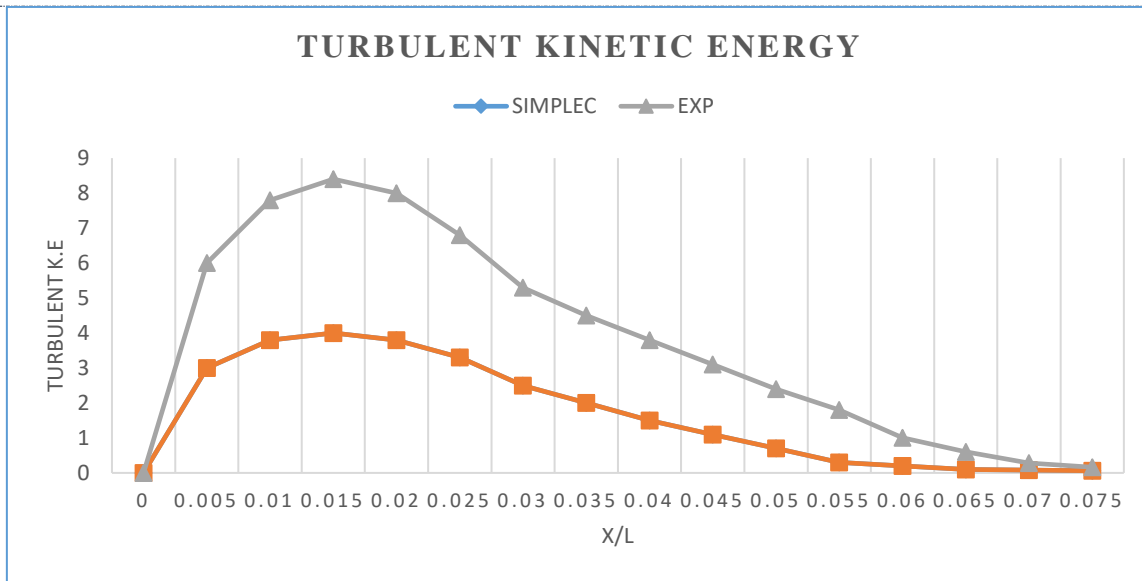
Fig. 7.6 Comparison of the Turbulent Kinetic Energy at y/H=0.5

Both the predicted and experimental profiles are asymmetrically distributed between the hot and cold walls and reach their maximum close to the hot wall given that turbulent kinetic energy varies with temperature gradients. The reason being shear stress, friction and buoyancy produces turbulence that causes an increase in fluctuating velocities near the hot surface. A comparison shows that the numerical prediction by SIMPLEC induced lower turbulence kinetic energy than the experimental results. In the core, at the middle section, there is very little activity and the turbulence level is very small. The reason being there is low temperature gradient hence low buoyancy, less friction and shear stress that is why the turbulent kinetic energy falls to zero.

Local Nusselt Number
Fig. 7.7 shows the heat transfer rate along the hot wall expressed in terms of the ratio of the convective to the conductive heat transfer across the boundary layer (local Nusselt number distribution). The SIMPLEC method over predicts Nusselt Number with a difference of 18%,
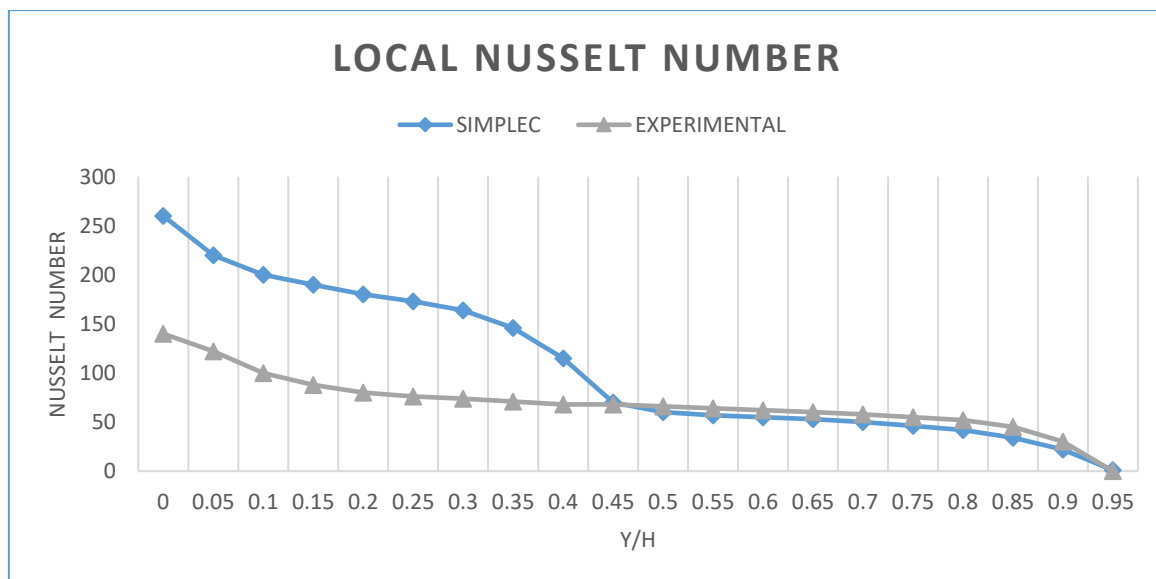

Fig. 7.7 Comparison of Local Nusselt Number along the Hot wall

on the lower half of the hot wall, then under-predicts it but weakly compared with the measured data on the upper part of the wall.

The over prediction of the Nusselt number in the initial parts of the hot surface may be related to the local minimum of temperature and residual cold draft coming over from the cold surface hence insufficient mixing between the laminar and turbulent core, which induces the sharper temperature gradient as seen and increases the convective heat transfer coefficient as seen in fig. 7.7.

Mean Vertical Velocity

Figure 7.8 shows the profiles for rate of change of vertical displacement of the fluid particles with time. The profiles are asymmetrical and with a peak near the heated surface.The rise is caused by the fluid gaining kinetic energy due to higher temperature gradient at the heated surface. The fall is due to (a) local minimum temperature (b) the cold drift coming over from cold wall. The two factors diminish the temperature gradient and make the kinetic energy in the fluid to dissipate.

As seen in figure 7.8, there is good agreement between the experimental data and the predicted data in terms of the mean velocity. The peak value of velocity is particularly well captured by SIMPLEC method. In the enclosure core region, there is very little activity and hence the fluid velocity is very small.
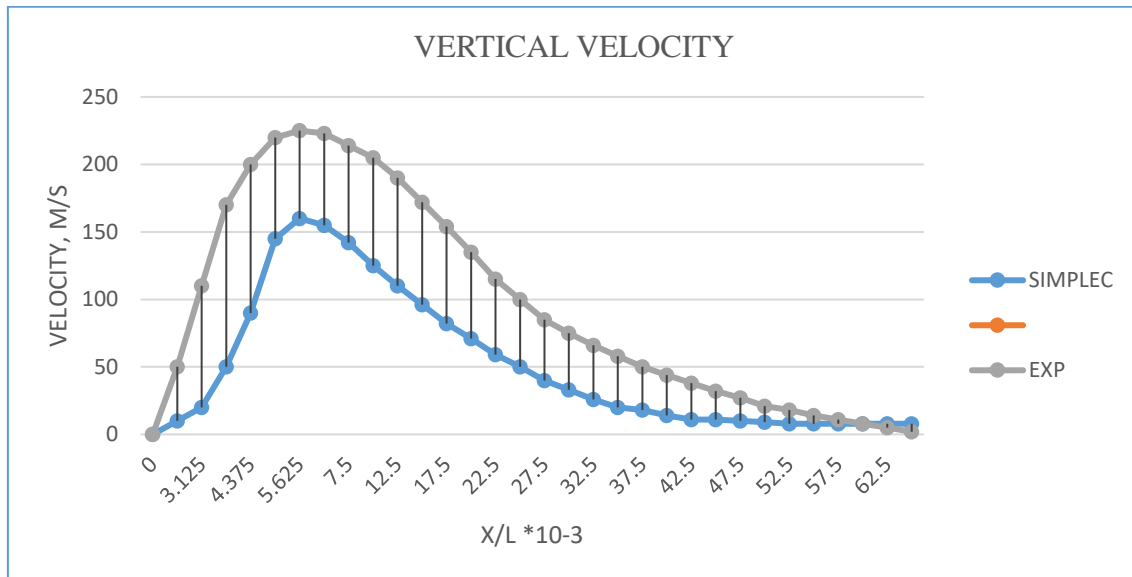

Fig. 7.8 Comparison of the vertical velocity

Mean Horizontal Velocity

Figure 7.9 shows the profiles of the rate of change of horizontal displacement of the fluid with time.
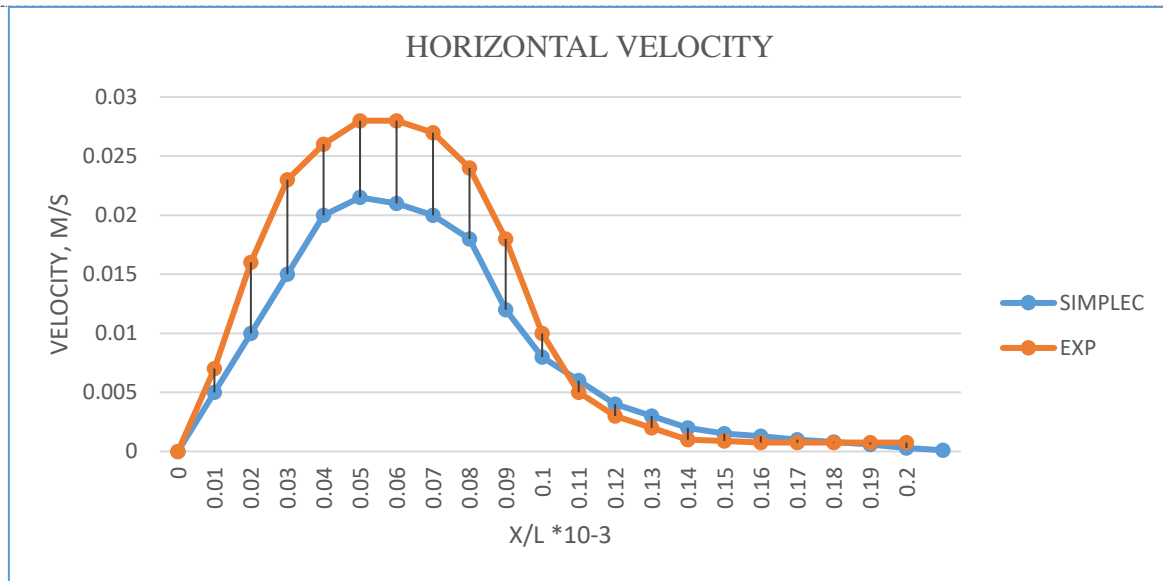
Fig. 7.9 Comparison of the Horizontal velocity

The rise of velocities near the heated surface of the cavity is as a result of fluid gaining kinetic energy from the heated wall causes an increased convective heat transfer coefficient, while the drop of velocities after 0.04 from the hot wallis as a result
(a) local minimum temperature
(b) the cold drift coming over from the opposite cold wall.

The two factors makes the energy in the fluid dissipate. All in all, there is good agreement between the experimental data and the predicted data in terms of the mean horizontal velocity, as in fig. 7.9

VIII.   CONCLUSION
  i)   From the numerical data, the numerical method produced a solution which approached the exact solution by Ampofo and Karayiannis (2003) as the grid spacing reduced to zero. Further, the method is stable, the governing equations consistent, as evidenced by the damping errors as the numerical method proceeded and the initial data did not cause wild oscillations of divergence.Therefore using Lax's equivalence theorem, Lax and Richtmyer (1956), this code is valid, stable and consistent.
  ii)   In this thesis, Both the experimental data and simulation using SIMPLEC return a non-dimensional temperature of 0.5 at the core of the cavity and almost zero towards the cold
         Therefore
      a)   The results show that in an enclosure environment, the natural turbulence flow is responsible for temperature distribution.
      b)   Temperature profiles are important for thermal comfort (including air velocity, temperature and humidity levels), efficiency of energy balance and the effectiveness of the ventilation system when modeling air flow in buildings.

IX.   ACKNOWLEDGEMENT
My sincere gratitude to Prof. F. K. Gatheri and Dr. G. W. Gachigua, for their contribution and inspiration.

X.   REFERENCES
  [1]   **Ampofo F. and Karanyiannis T. G. (2003)**, Experimental Benchmark Data for Turbulent Natural Convection in an Air-Filled Square Cavity, *Intenational Journal of Heat Mass Transfer*, **46**, 3551-3572
  [2]   **Awuor K. (2012)**, Turbulent Natural Convection in an Enclosure: Numerical Study of Different k-epsilon models, Ph.D. Thesis, Kenyatta University, Kenya, 1-102.
  [3]   **Berghein C., Penot F., Mergui S. and Allard F. (1993)**, Numerical and experimental evaluation of turbulent models for natural convection simulation in a thermally driven square cavity, *Proceedings on Adaptive Selection Mode Error Concealment (ASMEC) Conference*, 1-12.
  [4]   **Boussinesq J. (1903)**, *Th´eorie Analytique de la Chaleur, Gauthier-Villars*, **2**, 1-680

[5] **Davidson L. and Nielsen P.V. (1996)**, Large Eddy Simulations of the Flow in a Three- Dimensional Ventilated Room, *Proceedings Roomvent '96*, **2**, 161-168.

[6] **Dol H. S.and Hinjalic K.** (2001), Computational Study of Turbulent Natural Convention in a side Heated Near-cubic Enclosure at High Re, *International Journal of Heat and Mass Transfer*, **4**, 2323-2344

[7] **Gatheri F. K. (2005)**, Variable False Transient for the Solution of Coupled Elliptic Equations, East African Journal of Physical Sciences, **6** (2), 117

[8] **Gatheri F. K., Reizes J., Leonardi E. and Graham del Vahl Davis (1993)**, The use of Variable False Transient Factors for the Solution of Natural Convection Problems*, Australian Heat andMass Transfer*, University of Queensland, **5**, 68

[9] **Gatheri F. K., Reizes J., Leonardi E., and Graham del Vahl Davis (1994)**, Natural Convection in an Enclosure with Localized Heating and Cooling: A numerical Study, Heat Transfer 1994, G.F. Hewitt (ed), **2**, 361-366

[10] **Lax P. D. and Richtmyer R. D. (1956)**, Survey of the Stability of Linear Finite Difference Equations, *Communications on Pure and Applied Mathematics*, **9**, 267-293.

[11] **Pantaker S. V. (1980)**, Numerical Heat Transfer and Fluid Flow, Series in Computational Methods in Mechanics and Thermal Sciences, 1st Edition, Hemisphere Publishing Corporation, 25-39

[12] **Tian J. and Karayiannis T.G. (2001)**, Low turbulence natural convection in an air filled square cavity, J. Heat and Mass Transfer, **43**, 849-866

[13] **Tian, Y.S. and Karayianins, T.G. (2000)**, Low Turbulence Natural Convection in an Air Filled Square Cavity, Part I: The Thermal and Fluid Flow Fields. *International Journal of Heat andMass Transfer*, **43**, 849-866

CITE AN ARTICLE